

# Optics clues to pairing glues in high $T_c$ cuprates

**E. van Heumen, A.B. Kuzmenko, D. van der Marel**

Département de Physique de la Matière Condensée, Université de Genève, quai Ernest-Ansermet 24, CH1211, Genève 4, Switzerland

E-mail: [e.vanheumen@uva.nl](mailto:e.vanheumen@uva.nl)

**Abstract.** We analyze optical spectra of the high temperature superconductor  $\text{HgBa}_2\text{CuO}_{4+\delta}$  using a minimal model of electrons coupled to bosons. We consider the marginal Fermi liquid theory and the spin fluctuation theory, as well as a histogram representation of the bosonic spectral density. We find that the two theories can both be used to describe the experimental data provided that we allow for an additional scattering channel with an energy of 55 meV.

## 1. Introduction

The puzzle of superconductivity in the cuprates remains unsolved. Over the years it has become clear that the nature of the normal state is an equally important puzzle to solve. It now seems established that the strongly overdoped cuprates possess a well defined Fermi surface [1, ?, 2, ?] indicating that at least in this part of the phase diagram at low energy a Fermi liquid picture might apply for the normal state. The underdoped cuprates are characterized by so-called Fermi arcs: incomplete pieces of Fermi surface [?]. One might expect that in this part of the phase diagram the Fermi liquid paradigm is no longer appropriate and the physics is indeed described by that of a lightly doped anti-ferromagnetic insulator. Recent de Haas - van Alphen experiments however seem to indicate that the arcs should be interpreted in terms of small pockets [3] thus placing the state underlying the pseudogap state also in the Fermi liquid regime. Regardless the nature of the superconducting and normal state, the transition from one to the other is driven by the minimization of the free energy, which consists of potential ( $E_{pot}$ ) and kinetic energy ( $E_{kin}$ ). In conventional superconductors the transition is driven by a lowering of the potential energy while at the same time the formation of the Cooper pairs goes at the cost of a smaller amount of kinetic energy. Several experiments [4, 5, 6] have found that this situation might be different in the cuprates. In [4] the experimental results could be explained if it was assumed that superconductivity is driven by a gain in the  $c$ -axis  $E_{kin}$  while in the latter two cases the result can be interpreted in terms of a gain in  $ab$ -plane  $E_{kin}$ . In both cases it was argued that the different sign of  $E_{kin}$  with respect to conventional superconductors arises from the properties of the normal state (see i.e. Ref. [?] for the first case and Ref. [?, ?] for the second). In later experiments [7, 8, 9] the dependence of the change in  $E_{kin}$  on doping and the number of layers was studied. The results of these studies are summarized in figure 1. The quantity  $\Delta W$  is a measure of the kinetic energy change at the superconducting transition as defined in [10]. Interestingly,  $\Delta W$  changes sign for slightly overdoped samples. Assuming that the mechanism of superconductivity does not depend on doping, the sign change must arise from a change in the properties of the normal state.

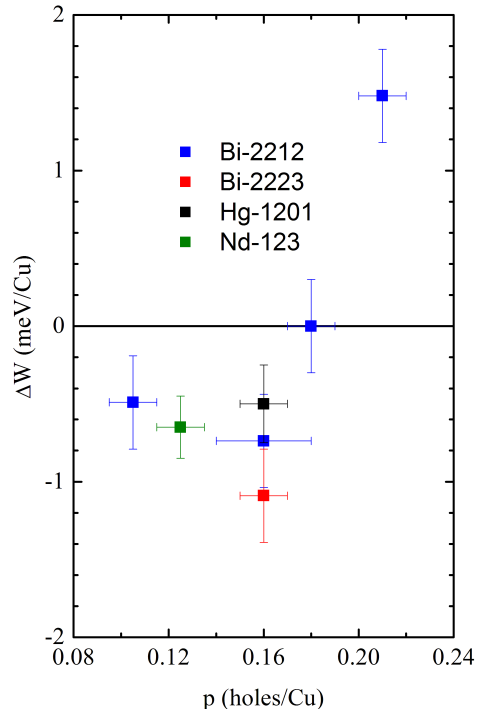


**Figure 1.** Doping dependence of the spectral weight change  $\Delta W$  at  $T_c$ . The numbers are taken from Ref. [5, 7] for Bi-2212, from Ref. [8] for Bi-2223 and from Ref. [9] for Hg-1201. The result for Nd-123 is unpublished. This result is similar to the one obtained by the group of Bontemps [?].

A possible interpretation of this result is that the superconducting dome covers a quantum critical point [?, 11]. In this scenario the underdoped and overdoped materials would be distinct phases explaining the change in Fermi surface topology and the change in sign of the superconductivity induced spectral weight. It has also been suggested that the optical properties of optimally doped Bi-2212 [12] and Bi-2223 [?] can be understood from quantum critical fluctuations. In [12] it was pointed out that at low energy the optical spectra could be described as a universal function of  $\omega/T$  while in the mid-infrared range the conductivity could be described by a powerlaw instead. However, as pointed out in [?] these two observations cannot be made consistent with each other without assuming a non-universal background to the optical conductivity.

Norman and Chubukov [13] showed that the powerlaw behavior could also have another interpretation: it follows that the optical conductivity has an approximate powerlaw behavior if one assumes a model in which electrons interact with a broad bosonic spectrum ( $\tilde{\Pi}(\omega)$ ). Using the same model the anomalously large temperature dependence of the normal state spectral weight could also be explained [14] but not the observed change in kinetic energy at  $T_c$  [?]. Stimulated by these positive results we analyzed the optical spectra of 10 different compounds using a histogram representation for the bosonic spectrum [?] and found that this spectrum strongly depends on doping and temperature. The doping dependence of  $\tilde{\Pi}(\omega)$  might give an explanation for the very different Fermi surfaces observed by ARPES for under- and overdoped cuprates, while the temperature dependence of the spectra could give an explanation for the (approximate)  $\omega/T$  scaling observed in [?]. Here we will discuss two possible models for the normal state and compare it to the earlier obtained histogram representation.

## 2. Methods

In normal metals the electron-phonon (EP) interaction can be described in a framework where fermionic quasiparticles, the electrons, interact with a spectrum of bosonic modes,

the phonons. The function describing the energy dependent coupling is often indicated as  $\alpha^2 F(\omega)$ . A closely related theory is the Eliashberg theory of superconductivity describing the occurrence of superconductivity in normal metals. It is an improvement of the BCS theory of superconductivity because it takes into account the retardation of the EP interaction.  $\alpha^2 F(\omega)$  also appears in this theory and is the main determining factor of the critical temperature at which superconductivity occurs. It is also possible to consider bosons other than phonons, for example plasmons, magnons or excitons. An important distinction between these bosons and phonons is that they are made up out of the same degrees of freedom which form the Cooper pairs: the electrons themselves.

We compare different models for the electron-boson coupling function, indicated here by the symbol  $\tilde{\Pi}(\omega)$ . The calculation of the optical conductivity for given  $\tilde{\Pi}(\omega)$  is straightforward (see Appendix A). The inverse problem of extracting  $\tilde{\Pi}(\omega)$  from experimental data can be done, but with limited accuracy due to the progression of errors due to experimental noise [15, 16]. Several theoretical models for the cuprates predict that the electrons interact with a bosonic spectrum.

### 2.1. Marginal Fermi liquid.

The Marginal Fermi Liquid (MFL) theory [17, 11] predicts that  $\tilde{\Pi}(\omega)$  is given by,

$$\tilde{\Pi}_{MFL}(\omega) = \Lambda \tanh\left(\frac{\omega}{2T}\right) f(\omega, \omega_c, \Delta) \quad (1)$$

where  $\Lambda$  is an overall coupling constant,  $T$  is the temperature and  $f(\omega, \omega_c, \Delta)$  is a high energy cutoff function the precise shape of which is unimportant. We have used  $f(\omega, \omega_c, \Delta) = 1/(1 + \exp(\frac{\omega - \omega_c}{\Delta}))$  as proposed originally by Varma [17]. An important feature of this spectrum is that it only depends on  $\omega/T$ . It is easy to see using Eq.'s A.1-A.4 that in this case one retrieves the linear temperature dependence of the resistivity seen in many experiments. It would also give rise to a conductivity that scales as  $\sigma(\omega, T) = T^{-1}g(\omega/T)$  as proposed in [?].

### 2.2. Spin fluctuation theory.

Several other theoretical models are based around the notion that anti-ferromagnetic fluctuations play an important role in understanding the physics of the (underdoped) cuprates [?, 18, ?]. In these models one uses the imaginary part of the dynamic spin susceptibility  $\chi''(\omega, \vec{q} = 0)$  as a measure for the bosonic spectral density which in the ungapped state is given by,

$$\tilde{\Pi}_{SF}(\omega) = \frac{\Gamma\omega}{\gamma^2 + \omega^2} \quad \omega \leq \omega_c \quad (2)$$

Here  $\Gamma$  is a coupling strength and  $\omega_c$  a cutoff. The spectrum has a maximum determined by  $\omega = \gamma$ . We refer to this model as the spin fluctuation (SF) model. Note that this form is valid only if there is no (pseudo)gap. Although the temperature dependence is not explicitly mentioned in Eq. 2 the parameters  $\gamma$  and  $\Gamma$  depend on temperature.  $\tilde{\Pi}_{SF}(\omega)$  does not scale as  $\omega/T$  unless both  $\gamma$  and  $\Gamma$  are depending linear on temperature. The temperature dependence of the MFL and SF models are an important point of contrast with the EP interaction which leads to a temperature independent  $\alpha^2 F(\omega)$ . The fact that most experimental studies find that for the cuprates  $\tilde{\Pi}(\omega)$  has to be made temperature dependent is one of the arguments against the interpretation of  $\tilde{\Pi}(\omega)$  in terms of phonons.

### 2.3. MFL and SF + phonon models

Finally we allow for a Lorentzian oscillator in addition to the MFL and SF model given by,

$$\tilde{\Pi}_{Lor}(\omega) = \frac{f_1^2 \Gamma_1 \omega}{(\omega \Gamma_1)^2 + (\omega_1^2 - \omega^2)^2} \quad (3)$$

Here  $f_1$  is the oscillator strength,  $\Gamma_1$  is the width and  $\omega_1$  is the center frequency. Such a peak can be used to describe the coupling of electrons to phonons or to the spin resonance.

#### 2.4. Histogram representation.

Although we cannot directly invert the experimental data to obtain  $\tilde{\Pi}(\omega)$  we can use a Levenberg-Marquardt optimization routine to determine the important features in  $\tilde{\Pi}(\omega)$ . We do this by making a histogram of  $\tilde{\Pi}(\omega)$  using  $i$  blocks with flexible widths and heights with a total of  $2i$  parameters,

$$\tilde{\Pi}_{HG}(\omega) = f_i \quad \omega_{i-1} \leq \omega \leq \omega_i \quad (4)$$

where  $\omega_0 = 0$  and  $f_i$  is the height of the  $i$ th block. We find that  $i=6$  is the optimal number of blocks giving sufficient detail to  $\tilde{\Pi}(\omega)$  without overdetermining it. For  $\omega_0 \leq \omega \leq \omega_1$  we use  $\Pi_{HG}(\omega) = f_1\omega$  to circumvent the divergence of the integral in Eq. A.2. The resulting histogram allows us to extract a rough impression of  $\tilde{\Pi}(\omega)$  and give an indication of the important features in the spectrum. This model function allows us to optimize  $\tilde{\Pi}(\omega)$  such that adding more detail does not significantly improve the result. This model was used in a recent study of 10 different compounds [?]. We showed that  $\tilde{\Pi}_{HG}(\omega)$  has three important features:

- $\tilde{\Pi}_{HG}(\omega)$  has to be temperature dependent.
- $\tilde{\Pi}_{HG}(\omega)$  extends to very high energies (about 400 meV) as compared to standard electron-phonon systems
- $\tilde{\Pi}_{HG}(\omega)$  is dominated by a peak (55 meV) in the phonon range.

The novel idea that follows from these observations is that the glue function of the cuprates is made up out of electronic and phononic contributions. Below we will come back to this point and try to estimate the separate contributions.

### 3. Results

We analyze optical spectra of optimally doped  $\text{HgBa}_2\text{CuO}_{4+\delta}$  (Hg-1201). This high temperature superconductor presents us with a good opportunity to test the above models without too many complications. It is a single layer compound with a simple tetragonal structure and it has a high critical temperature of  $T_c \approx 97$  K. The optical data has been presented before in Ref. [9]. We do not take into account the opening of a (pseudo-)gap in our analysis so we can only apply it to temperatures of 100 K and higher. Recent neutron scattering experiments [?] show that at optimal doping the pseudogap temperature is probably smaller or equal to the critical temperature for these materials at optimal doping, although specific heat measurements on the particular sample used in this study show an onset of the specific heat jump at slightly higher temperature [9]. In figure 2 we show the reflectivity for Hg-1201 together with the optimized model curves obtained with Eq.'s (1), (2) and (4). The corresponding spectral functions are shown in figure 3. Figure 2a and 3a show the results for the MFL model. At 290 K we can make a reasonable fit to the reflectivity but with decreasing temperature the fit becomes progressively worse. Note that we try to fit the overall frequency dependence of  $R(\omega)$  and not the sharper phonon structures below 80 meV. It is important to note that in order to optimize the mean squared deviation,  $\chi^2$  (see appendix), we have to make the coupling constant  $\lambda$  in Eq. 1 temperature dependent. This means that already at this level the  $\omega/T$  scaling is lost even for the MFL model. Our result obtained at room temperature is similar to that obtained in an earlier study [?]. We find that if we add an extra scattering channel to the MFL model the fit is greatly improved (see below).  $\tilde{\Pi}_{SF}(\omega)$  (panels 2b and 3b) shows a similar trend as seen for  $\tilde{\Pi}_{MFL}(\omega)$ : a reasonable fit at high temperature but less good at low temperature. Finally, figures 2c and 3c show  $\tilde{\Pi}_{HG}(\omega)$  which gives the best description of the optical data. The panels of figure 3 give a lot of information on the structure of  $\tilde{\Pi}(\omega)$ . As mentioned above it shows three

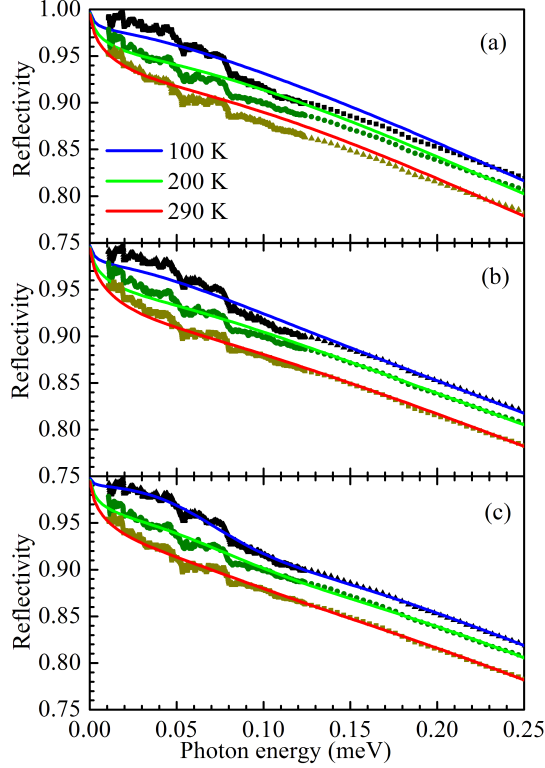


**Figure 2.** Reflectivity of Hg-1201 together with fits for three different models. (a): MFL model, (b): SF model and (c): histogram.

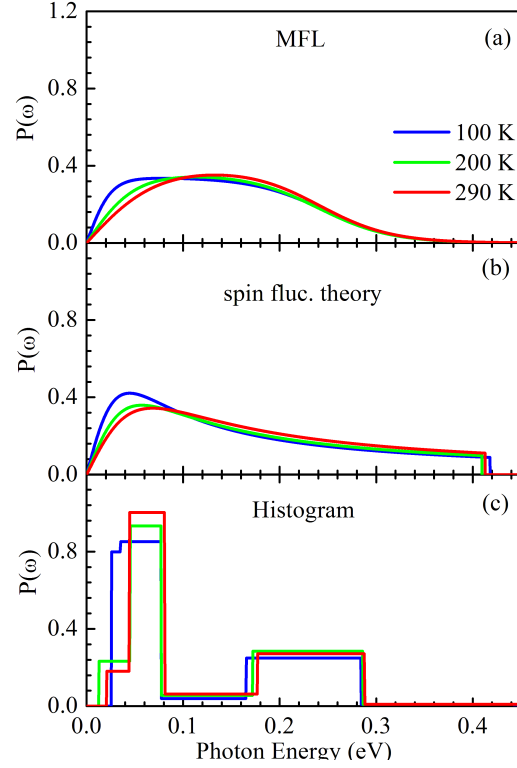


**Figure 3.** Temperature dependent spectral functions corresponding to the fits shown in the figure 2. (a): MFL model, (b): SF model and (c): histogram.

important features: (i)  $\tilde{\Pi}(\omega)$  has to be made temperature dependent. (ii) there is a high energy scale that is determined by the cutoff in  $\tilde{\Pi}(\omega)$  around 300 meV. (iii) there is a low energy scale determined by a maximum in  $\tilde{\Pi}(\omega)$  around 55 meV. We do not find evidence for  $\omega/T$  scaling of the function  $\tilde{\Pi}(\omega)$  from the above three model calculations. Even in the case of the MFL model we have to adjust the coupling constant  $\lambda$  for each temperature and this destroys the perfect  $\omega/T$  scaling.

To objectively compare the different models we use  $\chi^2$ , (Eq. A.5). Table 1 lists the optimized  $\chi^2$  for the fits shown in figure 2. From the table it follows that overall the SF model performs better than the MFL model. The reason for this is that the SF model has a maximum around 55 meV similar to the peak seen in the histogram representation. The MFL model in contrast has a broad maximum around 150 meV. The histogram representation suggests that  $\tilde{\Pi}(\omega)$  consists of two contributions: a peak on top of a broader continuum. In [?] we showed that this is true for a whole range of dopings and temperatures of single, double and triple layer cuprates. It is therefore tempting to ascribe the peak to oxygen vibrations present in this energy range while the continuum indicates coupling to either spin fluctuations or loop current excitations. There are different interpretations of our observations possible however.

A first possibility is that one of the assumptions underlying the strong coupling theory is simply no longer valid. In these materials the Fermi energy is quite small while the average mode energy is relatively high, which could mean that the Migdal approximation, which consists of neglecting vertex corrections, is no longer valid. This could mean that the high energy part of the background would be absent if these corrections are properly taken into account. However,

**Table 1.**  $\chi^2$  defined by Eq. A.5 for the three different models. The values in parentheses are obtained when a Lorentzian peak (Eq. 3) is added to the spectral function.

Model	290 K	200 K	100 K
MFL	117 (13)	127 (21)	163 (22)
SF	23 (15)	37 (21)	74 (18)
HG	11	19	13

Chubukov and Schmalian [20] considered 3D fermions coupled to a massless bosons spectrum and showed that vertex corrections can be neglected even in the strong coupling limit.

A second possibility is that we are interpreting parts of the electronic response in terms of  $\tilde{\Pi}(\omega)$  which is actually due to strong correlation effects. According to Anderson [21] the physics is determined by two energy scales: the antiferromagnetic exchange coupling  $J$  and the Hubbard repulsion  $U$ . Since  $J \approx 0.15$  eV it is possible that we are incorporating features in  $\tilde{P}i(\omega)$  which are actually related to RVB like fluctuations related to  $J$ .

The comparison of the panels in figure 3 suggests that we may get a better fit if we add a narrow peak to the MFL or SF model. As shown in table 1 the addition of this peak dramatically improves the quality of the fit, in particular for the MFL model. We can now easily separate the contribution due to the peak and the one due to the continuum which is not possible for the histogram representation. For each spectrum we can calculate the coupling constant which is given by,

$$\lambda = 2 \int_0^\infty \frac{\tilde{\Pi}(\omega)}{\omega} d\omega. \quad (5)$$

and separate the contribution from the 55 meV peak and the continuum. The total coupling constant at  $T = 290$  K from the histogram method is  $\lambda_{HG} = 1.85$  while  $\lambda_{MFL} = 1.9$  and  $\lambda_{SF} = 1.8$ . In the latter two cases the peak contributions are  $\lambda_{peak,MFL} = 0.88$  and  $\lambda_{peak,SF} = 0.65$  respectively. The peak energy is somewhat lower in energy than the low energy dispersion kink seen in ARPES experiments [?]. The coupling constants obtained by ARPES are of the order  $\lambda \approx 0.3 - 0.5$  [?, 22, ?, ?, 23] as are the coupling constants derived from LDA [?, ?]. The remaining coupling constant  $\lambda_{cont} \approx 1.2$  for the SF contribution also corresponds well with earlier estimates [?]. When the temperature is decreased the total coupling constant increases:  $\lambda_{200K} = 2.0$  and  $\lambda_{100K} = 2.3$ . Figure 3c indicates that this increase arises not simply from an increase in coupling to the mode but rather from an increase in intensity in the energy range below 50 meV. Since we cannot exclude pseudogap effects to play a role here we refrain from separating the contributions due to the mode and the background.

#### 4. Conclusion

We have presented a detailed analysis of optical spectra of the high temperature superconductor  $\text{HgBa}_2\text{CuO}_{4+\delta}$  in terms of strong coupling theory. A comparison of the marginal Fermi liquid model and the spin fluctuation model shows that the latter better describes the optical spectra of Hg-1201. However, the best description of the optical data is obtained when a low energy peak is added to either of the two models. A histogram model of  $\tilde{\Pi}(\omega)$  is dominated by a mode at 55 meV and this is lacking in the previous models. The addition of an extra mode to the MFL and SF models greatly improves the agreement with experiment for both models and allows us to separate the  $\tilde{\Pi}(\omega)$  spectrum into two components. The first is a nearly temperature independent peak centered at 55 meV with a coupling strength at room temperature  $\lambda_{mode} \approx$

0.7. The energy and coupling strength of this mode strongly suggest an interpretation in terms of electrons coupling to a vibrational mode. The second feature is a continuum with a maximum around 200 meV with a coupling strength of about  $\lambda_{cont} \approx 1.2$ .

## 5. Acknowledgements

We would like to acknowledge stimulating discussions with C.M. Varma, A.V. Chubukov and M.R. Norman, J. Zaanen, D.J. Scalapino and C. Berthod. This work is supported by the Swiss National Science Foundation through Grant No. 200020-113293 and the National Center of Competence in Research (NCCR) Materials with Novel Electronic Properties - MaNEP.

## Appendix A.

The calculation of the optical conductivity based on  $\tilde{\Pi}(\omega)$  rests on several assumptions. The most important are (i) the system is a Fermi liquid with a constant density of states, (ii) the electrons are coupled to bosonic modes that have little or no dispersion in k-space and (iii) one can ignore vertex corrections. For conventional superconductors these assumptions have been shown to be reasonable but they are not *a priori* correct when strong correlations effects are important. Calculations have shown that these assumptions still apply when the bosons are spin fluctuations with a spectrum that extends to relatively high energy in the strong coupling regime [20]. With the above approximations the complex optical conductivity  $\hat{\sigma}(\omega)$  can be expressed in terms of a self energy  $\Sigma(\omega)$  in the following way [24, 25],

$$\hat{\sigma}(\omega, T) = \frac{\omega_p^2}{i4\pi\omega} \int_{-\infty}^{+\infty} \frac{n_F(\omega + x, T) - n_F(x, T)dx}{\omega - \Sigma(x + \omega, T) + \Sigma^*(x, T) + i\Gamma_{imp}}, \quad (\text{A.1})$$

where  $\omega_p$  is the plasma frequency,  $\Gamma_{imp}$  is an impurity scattering rate,  $n_F(x) = (\exp(\beta x) + 1)^{-1}$  is the Fermi-Dirac distribution function and  $\beta = (k_b T)^{-1}$ . The self energy in Eq. A.1 is given by,

$$\Sigma(\omega, T) = \int d\varepsilon \int d\omega' \tilde{\Pi}(\omega') \left[ \frac{n_B(\omega') + n_F(\varepsilon)}{\omega - \varepsilon + \omega' + i\delta} + \frac{n_B(\omega') + 1 - n_F(\varepsilon)}{\omega - \varepsilon - \omega' - i\delta} \right] \quad (\text{A.2})$$

where  $n_B(x) = (\exp(\beta x) - 1)^{-1}$  is the Bose-Einstein distribution function. The integral over  $\varepsilon$  can be performed analytically, leaving,

$$\Sigma(\omega, T) = \int d\omega' \tilde{\Pi}(\omega') L(\omega, \omega', T). \quad (\text{A.3})$$

with

$$L(\omega, \omega', T) = -i\pi \coth\left(\frac{\omega}{2T}\right) + \Psi\left(\frac{1}{2} + i\frac{\omega - \omega'}{2\pi T}\right) - \Psi\left(\frac{1}{2} - i\frac{\omega + \omega'}{2\pi T}\right). \quad (\text{A.4})$$

The  $\Psi(x)$  in this last expression are digamma functions. Equations (A.1-A.4) together with the standard Fresnel equations allow us to calculate *any* optical property given  $\tilde{\Pi}(\omega)$ . From these equations one can also immediately see that it will be very difficult to extract  $\tilde{\Pi}(\omega)$  directly from the experimental data: this would require at least a second derivative of the optical data [15]. Given this difficulty we use the following approach. We choose an analytic form for  $\tilde{\Pi}(\omega)$  with several adjustable parameters and numerically perform the integrations in equations (A.1) and (A.3). The parameters of  $\tilde{\Pi}(\omega)$  are optimized using a standard Levenberg-Marquardt algorithm. This algorithm revolves around minimizing the function,

$$\chi^2 \equiv \sum_{i=1}^N \left( \frac{y_i - f(x_i, p_1, \dots, p_m)}{\sigma_i} \right)^2 \quad (\text{A.5})$$

where the  $y_i$  is the experimental datapoint value corresponding to the point  $x_i$  and  $f(x_i, p_1, \dots, p_m)$  is the calculated value in the point  $x_i$  from parameters  $p_1 \dots p_m$  that are to be optimized and the  $\sigma_i$  are the error bars on the value  $y_i$ . Since the optimization process requires knowledge of error bars on the quantity to be fitted, we use the reflectivity spectra measured in the infrared region of the spectrum for which we have accurate estimates of the error bars involved. Note that the calculation of the conductivity requires a choice for the plasma frequency,  $\omega_p$ . We add  $\omega_p$  as an independent fit parameter, but check that it is consistent with values obtained from a spectral weight analysis. The method described above applies to the intraband conductivity only. However, our spectra contain contributions due to interband transitions as well [9]. These we model using standard Lorentz oscillators added to the conductivity calculated using equation (A.1). A second point to be noted is that our analysis can only be carried out in the normal state. The analysis of spectra in the superconducting state is more challenging since it requires solving the full Eliashberg equations with high precision.

- [1] Hussey N E, Abdel-Jawad M, Carrington A, Mackenzie A P and Balicas L 2003 *Nature* **425** 814
- [2] Takeuchi T, Kondo T, Kitao T, Kaga H, Yang H, Ding H, Kaminski A and Campuzano J C 2005 *Phys. Rev. Lett.* **95** 227004 (pages 4)
- [3] Doiron-Leyraud N, Proust C, LeBoeuf D, Levallois J, Bonnemaïson J B, Liang R, Bonn D A, Hardy W N and Taillefer L 2007 *Nature* **447** 565–568
- [4] Basov D N, Woods S I, Katz A S, Singley E J, Dynes R C, Xu M, Hinks D G, Homes C C and Strongin M 1999 *Science* **283** 49–52
- [5] Molegraaf H J A, Presura C, van der Marel D, Kes P H and Li M 2002 *Science* **295** 2239–2241
- [6] Santander-Syro A F, Lobo R P S M, Bontemps N, Konstantinovic Z, Li Z Z and Raffy H 2003 *Europhys. Lett.* **62** 568–574
- [7] Carbone F, Kuzmenko A B, Molegraaf H J A, van Heumen E, Lukovac V, Marsiglio F, van der Marel D, Haule K, Kotliar G, Berger H, Courjault S, Kes P H and Li M 2006 *Phys. Rev. B* **74** 064510 (pages 8)
- [8] Carbone F, Kuzmenko A B, Molegraaf H J A, van Heumen E, Giannini E and van der Marel D 2006 *Phys. Rev. B* **74** 024502 (pages 10)
- [9] van Heumen E, Lortz R, Kuzmenko A B, Carbone F, van der Marel D, Zhao X, Yu G, Cho Y, Barisic N, Greven M and Dordevic C H S 2007 *Phys. Rev. B* **75** 054522 (pages 10)
- [10] Kuzmenko A B, Molegraaf H J A, Carbone F and van der Marel D 2005 *Phys. Rev. B* **72** 144503 (pages 9)
- [11] Aji V and Varma C M 2007 *Phys. Rev. Lett.* **99** 067003 (pages 4)
- [12] van der Marel D, Molegraaf H J A, Zaanen J, Nussinov Z, Carbone F, Damascelli A, Eisaki H, Greven M, Kes P H and Li M 2003 *Nature* **425** 271–274
- [13] Norman M R and Chubukov A V 2006 *Phys. Rev. B* **73** 140501 (pages 4)
- [14] Norman M R, Chubukov A V, van Heumen E, Kuzmenko A B and van der Marel D 2007 *Phys. Rev. B* **76** 220509 (pages 4)
- [15] Marsiglio F, Startseva T and Carbotte J 1998 *Phys. Lett. A* **245** 172
- [16] Dordevic S V, Homes C C, Tu J J, Valla T, Strongin M, Johnson P D, Gu G D and Basov D N 2005 *Phys. Rev. B* **71** 104529 (pages 12)
- [17] Varma C M, Littlewood P B, Schmitt-Rink S, Abrahams E and Ruckenstein A E 1989 *Phys. Rev. Lett.* **63** 1996–1999
- [18] Millis A J, Monien H and Pines D 1990 *Phys. Rev. B* **42** 167–178
- [19] Li Y, Baldent V, Barisic N, Cho Y, Fauqu B, Sidis Y, Yu G, Zhao X, Bourges P and Greven M *cond-mat:0805.2959*
- [20] Chubukov A V and Schmalian J 2005 *Phys. Rev. B* **72** 174520 (pages 14)
- [21] Anderson P W 2007 *Science* **316** 1705–1707
- [22] Lanzara A, Bogdanov P V, Zhou X J, Kellar S A, Feng D L, Lu E D, Yoshida T, Eisaki H, Fujimori A, Kishio K, Shimoyama J I, Noda T, Uchida S, Hussain Z and Shen Z X 2001 *Nature* **412** 510
- [23] Meevasana W, Ingle N J C, Lu D H, Shi J R, Baumberger F, Shen K M, Lee W S, Cuk T, Eisaki H, Devereaux T P, Nagaosa N, Zaanen J and Shen Z X 2006 *Phys. Rev. Lett.* **96** 157003 (pages 4)
- [24] Allen P B 1971 *Phys. Rev. B* **3** 305–320
- [25] Allen P B and Mitrovic B 1982 *Solid state physics* Advances in research and applications ed Ehrenreich H, Seitz F and Turnbull D (London: Academic Press) p 2